Osteoarthritis and Cartilage 25 (2017) 413–420

Osteoarthritis and Cartilage

The use of a cartilage decellularized matrix scaffold for the repair of osteochondral defects: the importance of long-term studies in a large animal model

R.A. Vindas Bolaños †, S.M. Cokelaere ‡, J.M. Estrada McDermott †, K.E.M. Benders §, U. Gbureck ||, S.G.M. Plomp ‡, H. Weinans §, J. Groll ||, P.R. van Weeren ‡, J. Malda ‡ § *

† *Cátedra de Cirugía de Especies Mayores, Escuela de Medicina Veterinaria, Universidad Nacional, Heredia, Costa Rica*
‡ *Department of Equine Sciences, Faculty of Veterinary Medicine, Utrecht University, The Netherlands*
§ *Department of Orthopaedics, Division of Surgery, University Medical Center Utrecht, Utrecht, The Netherlands*
|| *Department of Functional Materials in Medicine and Dentistry, University of Würzburg, Würzburg, Germany*

ARTICLE INFO

Article history:
Received 28 April 2016
Received in revised form
15 July 2016
Accepted 11 August 2016

Keywords:
Animal models
Cartilage
Scaffolds
Equine model
Long-term study
Osteochondral defect

SUMMARY

Objective: To investigate the effect of decellularized cartilage-derived matrix (CDM) scaffolds, by itself and as a composite scaffold with a calcium phosphate (CaP) base, for the repair of osteochondral defects. It was hypothesized that the chondral defects would heal with fibrocartilaginous tissue and that the composite scaffold would result in better bone formation.

Methods: After an 8-week pilot experiment in a single horse, scaffolds were implanted in eight healthy horses in osteochondral defects on the medial trochlear ridge of the femur. In one joint a composite CDM–CaP scaffold was implanted (+P), in the contralateral joint a CDM only (−P) scaffold. After euthanasia at 6 months, tissues were analysed by histology, immunohistochemistry, micro-CT, biochemistry and biomechanical evaluation.

Results: The 8-week pilot showed encouraging formation of bone and cartilage, but incomplete defect filling. At 6 months, micro-CT and histology showed much more limited filling of the defect, but the CaP component of the +P scaffolds was well integrated with the surrounding bone. The repair tissue was fibrotic with high collagen type I and low type II content and with no differences between the groups. There were also no biochemical differences between the groups and repair tissue was much less stiff than normal tissue ($P < 0.0001$).

Conclusions: The implants failed to produce reasonable repair tissue in this osteochondral defect model, although the CaP base in the −P group integrated well with the recipient bone. The study stresses the importance of long-term *in vivo* studies to assess the efficacy of cartilage repair techniques.

Introduction

In the quest for techniques to produce a cartilage repair tissue that will remain functional life-long, a wide range of approaches have been explored[1]. Although some techniques, such as various variants of autologous chondrocyte implantation (ACI)[2] and joint distraction[3], yield promising clinical results, none of these approaches has yet been proven to fully restore proper hyaline cartilage. An alternative technique that has yielded very promising results in other areas of regenerative medicine, such as restoration of bladder, trachea and gut, is the use of scaffolds based on decellularized extracellular matrix (ECM)[4]. The advantage of this technique is that an environment of natural ECM elements is created that may still contain a variety of appropriate bioactive cues without the presence of cellular components, hence avoiding immunological issues[5,6]. Moreover, it does allow for a xenogenic approach as ECM proteins are highly conserved across species[4]. *In vitro* studies have already demonstrated the potential of cartilage-derived matrix (CDM) scaffolds, as abundant new glycosaminoglycan (GAG)- and collagen type II-containing cartilaginous matrix was formed by cultured mesenchymal

* Address correspondence and reprint requests to: J. Malda, Department of Equine Sciences, Faculty of Veterinary Medicine, Utrecht University, The Netherlands.
E-mail address: j.malda@umcutrecht.nl (J. Malda).

http://dx.doi.org/10.1016/j.joca.2016.08.005
1063-4584/

stromal cells[7]. The potency was further underscored by *in vivo* studies in small animal models both at ectopic[6,8] and orthotopic locations[9,10].

The CDM scaffolds are potentially interesting for the repair of osteochondral defects, as they can be custom-shaped into osteochondral plugs that can be inserted in a press-fit fashion, avoiding insecure or complicating fixation techniques that may induce damage to the surrounding and opposing tissue[11]. They also have the potential to become an off-the-shelf product, as there is no need for pre-implantation culturing. This approach, however, requires the simultaneous regeneration of both bony and cartilaginous tissues. This can in theory be realized by using either a composite scaffold, or a single scaffold that will allow formation of both tissues, depending on the surrounding original tissue.

In this study, a CDM-based scaffold is developed and used. The CDM consists of predominantly collagen type II, in the absence of GAGs and cells[12] and is used either on its own, or combined with a three-dimensionally (3D) printed calcium phosphate (CaP) cement-based proven osteogenic scaffold[13,14] to fill osteochondral defects in the femoropatellar joints of horses. The equine model is seen as one of the best and most challenging models for orthopaedic ailments[15,16]. It was hypothesized that the chondral portion of the osteochondral defects would heal with neo-tissue coming close to hyaline cartilage and that the composite scaffold would show better bone formation and lead to better overall anatomical reconstitution.

Methods

Animals

The protocols and studies described were approved by the ethical and animal welfare committees of Utrecht University (pilot study) and National University of Costa Rica (long-term study). For the pilot study one Dutch Warmblood horse (age: 6 years, 490 kg) was used, while for the long-term study eight healthy Criollo breed horses (age 4–9 years; weight 275–350 kg) were used. The horses were free of lameness and without any clinical or radiographic evidence of acute or chronic injuries. They were housed in individual boxes, and fed a standard maintenance ration of concentrate with hay *ad libitum* and free access to water.

Scaffold preparation

Full-thickness cartilage was harvested from cadaveric femoropatellar joints of horses ($n = 5$; age 3–10 years), euthanized for reasons other than joint disease, with owner permission. The cartilage particles were pooled and decellularized according to a protocol previously described[11]. Finally, particles were milled in liquid nitrogen (A11 basic analytical mill, IKA, Staufen, Germany) and sieved through pores of 300 μm.

The CaP scaffold [Fig. 1(A), (B)] was manufactured by 3D printing of tricalcium phosphate (TCP) powder with diluted phosphoric acid, as described previously[14]. Briefly, TCP was synthesized by heating a mixture of $CaHPO_4$ and $CaCO_3$ (both Merck, Germany) in a 2:1 molar ratio to 1400°C for 5 h, followed by quenching to room temperature. The sintered cake was manually crushed and sieved <125 μm and finally ground in a ball mill (PM400, Retsch, Germany) for 10 min. Printing was performed on a Z-Corp 310 powder printer (Z-Corporation, Burlington, USA) by using the TCP powder and 20 wt% phosphoric acid as printing liquid.

The suspended decellularized particles were placed in a 11 mm diameter cylindrical mould, either directly (−P) or placed on top of the CaP scaffolds (+P) while ensuring that they penetrated all macropores of the CaP scaffold. The scaffolds were then lyophilized for 24 h and subjected to ultraviolet light overnight to allow for crosslinking, before sterilization using ethylene oxide gas.

Experimental design

Scaffolds were implanted in 11 mm diameter and 10 mm deep cylindrical defects that were surgically created at the axial side of the medial femoral trochlear ridge. The 8-week pilot study was performed to evaluate the short-term response to the CDM scaffold. To reduce the use of experimental animals, a horse was used that was destined to be sacrificed for educational purposes. No CaP scaffold was used in this case. In the main 6-month study, each horse received both the treatment with CDM scaffold alone (−P) and with a composite scaffold consisting of CDM and a 3D printed CaP scaffold (+P). Horses 1–4 received treatment −P and +P for the left and right femoropatellar joints, respectively. For horses 5–8 this was inverted.

Surgical procedure

After premedication with xylazine (1.1 mg/kg, Pisa) intravenously (IV), horses were induced with ketamine (2.2 mg/kg, Holliday) and midazolam (0.05 mg/kg, Holliday) IV and positioned in dorsal recumbence. General anaesthesia was maintained with isoflurane in oxygen.

A cranial femoropatellar mini-arthrotomy was performed through a 5 cm incision made between the middle and medial patellar ligaments[17]. Osteochondral defects at the middle aspect of each medial femoral trochlear ridge were created using a power-driven drill. Defect site and joints were flushed with saline solution (Careflex) before implantation. Scaffolds were press-fit implanted into each defect. Wounds were sutured in four layers (joint capsule, deep fascia, superficial fascia, and skin) and a stent bandage was applied over the incision.

Post-operative care and rehabilitation

Post-operatively, horses received antibiotics for 8 days (procaine penicillin 15,000 IU/kg intramuscularly SID, Alfasan, and IV gentamicin 6.6 mg/kg BID, Alfasan), and non-steroidal anti-inflammatory drugs (phenylbutazone (2.2 mg/kg, Lisan, orally BID)) during the first 14 days.

The pilot horse was subjected to the following rehabilitation protocol during the next 8 weeks: from week 2, the horse was hand-walked daily starting with 5 min/day with increments of 5 min per week until 20 min/day was reached. In the main study, from week 3, horses were hand-walked starting with 5 min/day with increments of 5 min/week, until 30 min/day was reached, which was then kept stable until week 16. In months 5 and 6, horses were walked, trotted and cantered for 2 min at each gait.

Monitoring during experimental period

The animals were subjected to daily monitoring of clinical parameters (temperature, heart rate and respiratory rate). Blood parameters were checked and lateromedial radiographs of the femoropatellar joints were taken before surgery and at months 1, 2, 4 and 6 after the intervention to check for general health.

Euthanasia and sample harvesting

The pilot horse was euthanized at 8 weeks by a combination of detomidine (0.01 mg/kg, Vetoquinol), ketamine (2 mg/kg, Vetoquinol), midazolam (0.1 mg/kg, Actavis) and pentobarbital (50 mg/kg, AST Farma). The horses of the main study were euthanized at 6

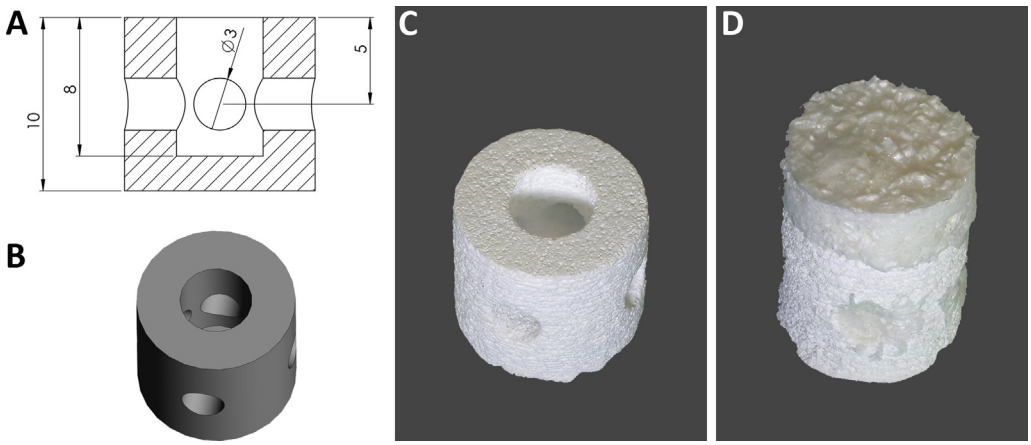

Fig. 1. Macroscopic views of scaffolds. The 3D design (A; all distances in mm), rendering (B) and printed CaP scaffold (C), which was subsequently combined in a mould with the CDM scaffold (D).

months using a combination of xylazine (1 mg/kg IV, Pisa) and ketamine–midazolam (3 mg/kg–0.05 mg/kg IV, Holliday) to induce profound anaesthesia. After this, a bolus of oversaturated magnesium sulphate (200 g/l) and chloral hydrate (200 g/l) solution was administered to effect.

After opening the femoropatellar joint, macroscopic pictures were taken and blocks of tissue containing the defect were excised. A piece containing one half of the treated defect was fixed in 10% formalin for micro-CT analysis and histological evaluation after embedding in polymethylmethacrylate (MMA). The remainder of the tissue was snap-frozen in liquid nitrogen and stored at −80°C until further processing for paraffin-based histological, biomechanical and biochemical analyses.

Micro-CT imaging and CaP scaffold analysis

To visualize the calcified tissue at the defect site, the formalin-fixed tissue underwent micro-CT analysis (Quantum FX-Perkin Elmer) with scan parameters 90 kV tube voltage, 180 mA tube current, 60 μm resolution and 3 min scan time. Reconstruction of 2D projections was automatically performed using the inbuilt software; image calibration and noise reduction was undertaken with Analyze-11.0 software.

Remnants of CaP scaffolds were analysed by XRD analysis (D5005, Siemens, Karlsruhe, Germany) using monochromatic Cu $K_{\alpha 1}$ radiation in a 2Theta range of 20–40° with a step size of 0.02°. Diffraction patterns were qualitatively analysed using the following reference patterns from the powder diffraction database: brushite (PDF-No. 09-0077), monetite (PDF-No. 09-0080), β-tricalcium phosphate (β-TCP) (PDF-No. 09-0169), α-tricalcium phosphate (α-TCP) (PDF-No. 09-0348) and hydroxyapatite (HA) (PDF-No. 09-0432).

Biomechanical testing

Micro-indentation experiments were performed on both healthy cartilage and defect tissue from the same animal. A displacement-controlled nano-indenter machine (Piuma, the Netherlands) with a spherical indenter (radius: 73 μm, cantilever stiffness: 15.6 N/m) was used to obtain indentation-based load–displacement curves[18]. A 3 × 3 matrix of indentation ($n = 9$) covering 600 × 600 μm^2 area, corresponding with 300 μm distance between each point, was performed. The actual indentation depth was in the range of 8 microns. The Young's modulus was calculated based on the Oliver–Pharr theory using the initial slope of the unloading curve and estimated Poisson's ratio of 0.5[19].

After biomechanical testing, half of the sample was fixed in formalin and further processed for paraffin embedding. From the remaining tissue sample, the soft tissue of the defect was excised and processed for biochemical analysis.

Histological processing

Formalin-fixed samples were embedded in MMA and cut with a Leica 4 SP1600 Saw Microtome system (Leica, Germany) to yield 20–30 μm sections. Sections were stained with methylene blue (Merck, 1.06045)/basic fuchsine (Klinipath, 800561).

Former frozen tissue samples were, after fixation in 10% formalin, decalcified in ethylene diamine tetra acetic acid (EDTA) and dehydrated through a graded ethanol series, cleared in xylene, embedded in paraffin, and sectioned (5 μm). To visualize cells, sections were stained with haematoxylin (Klinipath) and eosin (Merck, 115935). To visualize collagen fibre orientation, a picrosirius red staining (Klinipath, 80115) was performed. A triple stain of haematoxylin, fast green, and Safranin-O (both from Sigma) was also applied to identify the presence of GAGs. Stained sections were examined using a light microscope (Olympus BX51). Immunohistochemistry was used to identify collagen type I (Rabbit monoclonal from Abcam (AB138492); 1:500 dilution) and II (Mouse monoclonal Antibody DSHB, II-II6B3; 1:1500 dilution) after deparaffinization and rehydration of the sections following a protocol described previously[6].

Biochemical analyses

Tissue derived from the defect area after biomechanical testing was used for DNA, GAG and hydroxyproline (HYP) quantification. Samples were digested overnight in papain solution, 200 ml per sample (0.01 M cysteine, 250 μg/ml papain, 0.2 M NaH_2PO_4 and 0.01 M EDTA) at 60°C. Total DNA was quantified on the papain digest using the Qubit 2.0 fluorimeter with the Qubit dsDNA BR Assay Kit (Q32853) according to the manufacturer's instructions. Total GAG content was determined after reaction with dimethyl methylene blue as described previously[8]. Collagen was quantified by using a HYP assay. Samples were freeze-dried overnight and hydrolysed at 108°C overnight in 4 M NaOH. HYP was measured after reaction with Dimethylaminobenzaldehyde, the absorbance was read at 570 nm using a microplate reader (Tecan).

Statistics

Data are presented as mean and confidence interval. Statistical significance was determined, using SPSS software, for biochemical and biomechanical quantification a paired *t*-test was used, and for biomechanical testing a Wilcoxon signed ranks test was used.

Results

Scaffold preparation

The composite scaffold consisted of the CaP custom-designed 3D printed base [Fig. 1(A)–(C)], to promote bone regeneration, and the CDM scaffold [Fig. 1(D)] for the restoration of the cartilage compartment. After lyophilisation a good integration of the CDM scaffold was obtained and the CDM compartment was trimmed to 2 mm allowing for good accessibility of internal pores.

Pilot experiment

The horse in the pilot experiment recovered well from anaesthesia and had an uneventful post-operative period. At 8 weeks, an indentation of the cartilage surface was observed macroscopically, but regeneration of both the bone and cartilage phase was evident at a microscopic level [Fig. 2(A)]. There was excellent integration of newly formed trabecular bone with the original subchondral bone. There was intense staining for proteoglycans [Fig. 2(A)] and collagen type II [Fig. 2(B)] and there were indications for integration with the pre-existent tissue at the margins of the defect at this level. Nevertheless, the cartilage phase showed some cleft formation and disorganisation of collagen structures, as evidenced by picrosirius red staining [Fig. 2(C)] and was positive for collagen type I (data not shown).

Surgery and clinical and radiographic observations during experimental period

For the 6-month study, horses recovered uneventfully and could cope well with the post-surgical rehabilitation period. After the initial recovery period, no significant lameness was observed in six of eight horses. The remaining two showed intermittent mild lameness that responded well to treatment with non-steroidal analgesics. In all horses, clinical and blood parameters remained within normal physiologic limits. The radiographs taken at 2 months after surgery showed evidence of the artificial defects, with a clear difference between the sides treated with −P and +P implants (Suppl. Fig. 1). Whilst the +P scaffolds had a radio dense appearance [Suppl. Fig. 1(B)], around the −P scaffolds a sclerotic rim was visible [Suppl. Fig. 1(D)].

Macroscopic appearance at necropsy

At the time of euthanasia, the surgical sites were readily recognizable by an indentation in the cartilage (Fig. 3); whilst at the time point of implantation implants had been carefully placed level with the surrounding cartilage. All sites had a similar appearance without macroscopically visible differences between treatments.

Micro-CT and analysis of the CaP scaffold

Micro-CT analyses showed that filling of the bony part of the defect was very limited and considerably less than observed in the *in vivo* pilot experiment in all cases, although the CaP component of the +P scaffolds appeared well integrated with the surrounding bone (Fig. 4). Prior to implantation, the 3D printed scaffolds were composed of a mixture of brushite ($CaHPO_4 \cdot 2H_2O$), monetite ($CaHPO_4$), β-TCP and α-TCP. Analysis of the remnants of the retrieved CaP scaffold by XRD showed that most of the scaffolds had dissolved during the implantation period since no brushite, monetite and α-TCP could be detected in all samples. Only in few cases, small residues of crystalline β-TCP could be found. All analysed samples contained nanocrystalline HA, which either originates from direct conversion of brushite (or α-TCP), or it stems from newly formed bone matrix [Fig. 4(E)].

Biomechanical analysis

Biomechanical testing showed that the repair tissue in both −P and +P treated defects was very soft (mean Young's modulus 302 KPa (CI 177–427) for −P and 261 KPa (CI 148–374) respectively) and the stiffness was significantly less than that of normal adjacent cartilage (mean Young's modulus for −P 2385 KPa (CI 2009–2761), for +P

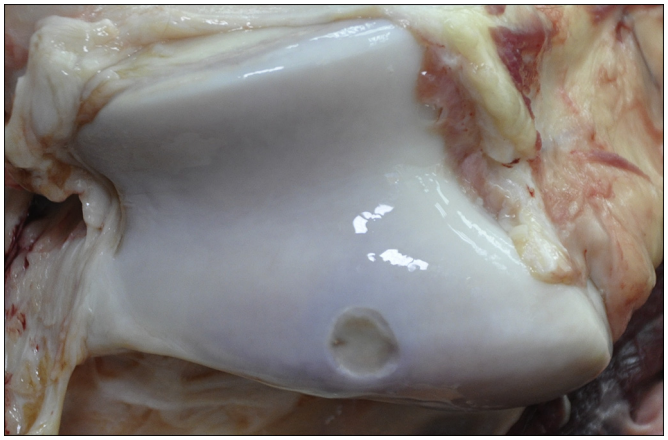

Fig. 3. Macroscopic view of the surgical site at necropsy (6 months after implantation).

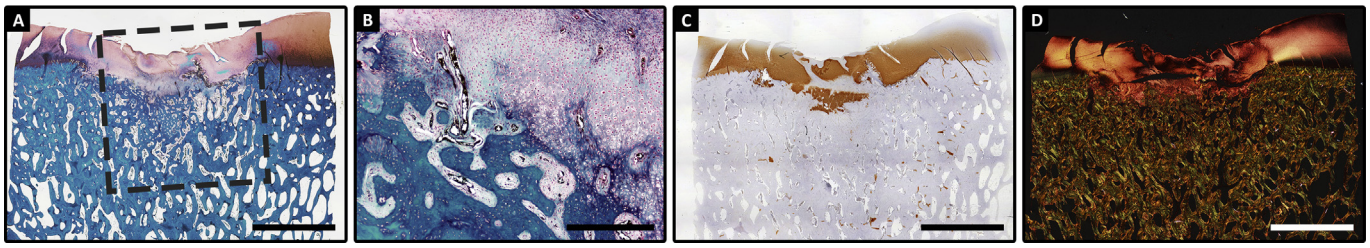

Fig. 2. Histological view of the artificial defect treated with a decellularized CDM scaffold after 8 weeks. Newly formed tissue was rich in GAGs (GAGs stain red with safranin-O (A)); and rich in collagen type II (brown in B) with clear distinction between cartilage and bone phases. Picrosirius red staining demonstrates under polarized light the disorganisation in the collagen fibril organisation (C). Scale bars represent 500 μm.

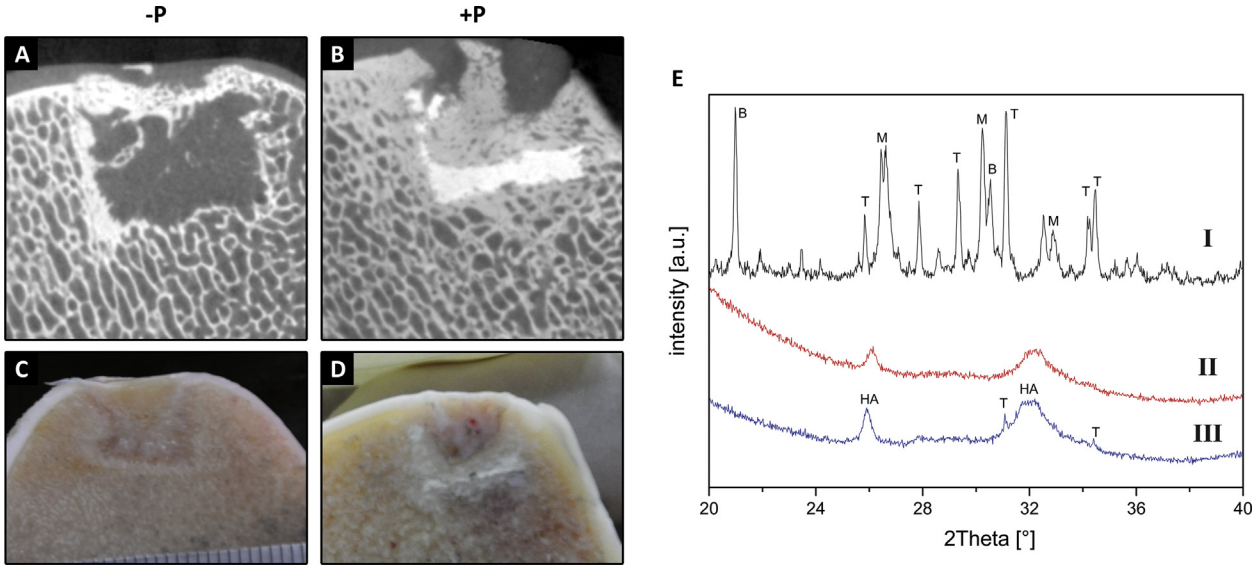

Fig. 4. Micro-CT and macroscopic pictures, respectively, of implantation sites at 6 months for −P (A, C) and +P (B, D) scaffolds. XRD analysis of 3D printed CaP scaffolds (E); I indicates a sample before implantation, whilst II and III indicate samples at necropsy. The most prominent peaks are labelled as: B: brushite (PDF-No. 09-0077), M: monetite (PDF-No. 09-0080), T: β-tricalcium phosphate (PDF-No. 09-0169) and HA: hydroxyapatite (PDF-No. 09-0432).

2372 KPa (CI 2036–2708) ($P < 0.0001$)). There was no difference between repair tissue of the −P and +P groups ($P > 0.05$) (Fig. 5).

Biochemistry

In line with the histological observations, there was limited GAG production in the defects. Values for GAG, DNA and GAG/DNA for the −P condition were 25.67 (CI 17.27–34.07) μg/mg tissue, 1.57 (CI 1.35–1.79) μg/mg tissue and 16.54 (CI 12.09–20.99) respectively. For −P these were 12.32 (CI 9.88–14.82); 1.74 (CI 1.63–1.85) and 7.13 (CI 6.63–8.63) respectively. For the collagen parameter HYP values were 11.63 (CI 10.47–12.79) and 8.78 (CI 7.03–10.53) Hyp/mg tissue. There were no significant differences in the GAG and collagen content between the −P and +P groups (Fig. 6).

Histology

Histological staining of paraffin-embedded samples from the edges of both +P and −P treated defects demonstrates that a predominantly fibrotic repair tissue had been formed (Fig. 7) without obvious differences between the groups. The neo-tissue contained very limited amounts of GAGs and collagen type II, while abundant staining for collagen type I was observed (Suppl. Fig. 2).

The MMA sections showed substantial retention of the CaP scaffold at 6 months [Fig. 8(A)] with good to very good adherence of the surrounding trabecular bone to the scaffold [Fig. 8(B)].

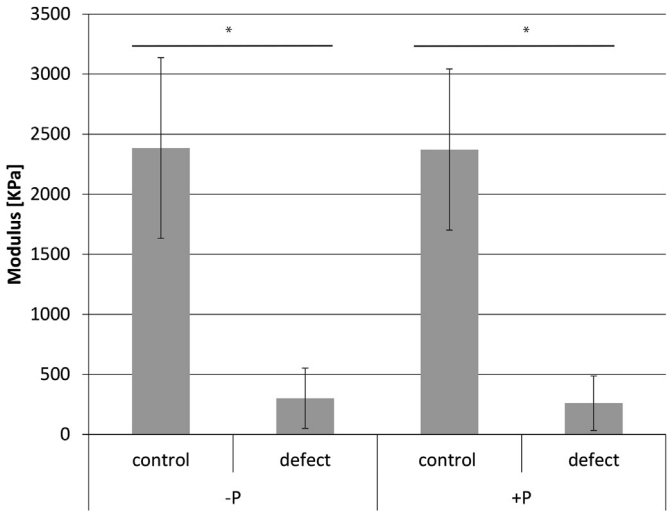

Fig. 5. Young's modulus of repair tissue vs normal cartilage from lesions treated with CDM only (−P) or CDM plus CaP scaffolds (+P). *$P < 0.0001$, $n = 8$ for all groups.

Discussion

Since the early days of tissue engineering, articular cartilage has been one of the target tissues[22]. It however soon became clear that extensive *in vitro* testing in the classic smaller laboratory species, while still being of absolute necessity in the initial developmental phase, were not sufficient for evaluation of any therapy aiming at cartilage repair or regeneration in clinical circumstances[23]. Of the larger models, the equine model is regarded as one of the best, but also as one of the most challenging[16]. Advantages include the size and accessibility of the joints, the thickness and biochemical composition of the cartilage, which are close to those in humans[24], and the fact that the subchondral plate is closed, which is not the case in many of the smaller species. Among the disadvantages of the model perhaps the immediate load-bearing after surgery may be most important[25]. An important ethical consideration with respect to the equine model is that horses are animals that are primarily bred and kept for their athletic potential. This makes the horse, unlike any other species with the possible exception of the dog, into an experimental species, as well as a target species, with a clear clinical need for better treatment of (osteo)chondral articular disorders[26].

In this study, the equine model was used to evaluate the effect of filling an artificial osteochondral defect with a cell-free CDM scaffold, with (+P) or without (−P) a ceramic base for press-fit anchoring in the subchondral bone. Results of the implantation of a CDM only implant in the 8-week pilot study were in line with previous promising results from *in vivo* ectopic studies with these scaffolds[6,8], as well as the orthotopic implantations in rabbits[9,10]. At the site of the scaffold, regeneration of both the bone and cartilage phase were seen, although a marked indentation of the articular

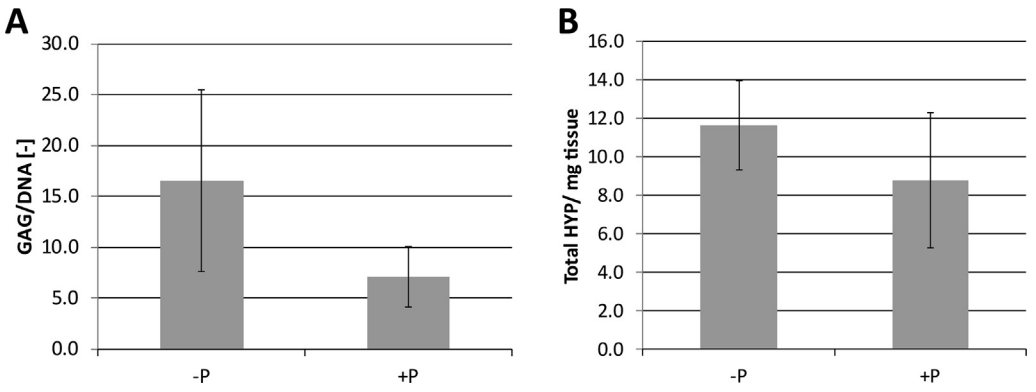

Fig. 6. Average GAG (A) and hydroxyproline (HYP, μg/mg dry weight; (B) content, as a measure of collagen content, of the repair tissue after 6 months.

surface could be noted. Nevertheless, the outcome of the pilot study was deemed encouraging enough to justify a larger longer-term study.

While in the main study clinical signs, such as lameness or joint effusion, were limited and not seen in all horses, defect filling at necropsy at 6 months was disappointing and clearly less than in the pilot horse in all treated animals. Macroscopic and histological analysis confirmed large indentations and the presence of inferior repair tissue. Biomechanically, this tissue was on average 90% less stiff than samples from healthy cartilage from the same horse. In contrast, the 3D printed CaP cement from the bony part of the scaffold was well integrated in the surrounding bone tissue, similar to previous orthotopic studies[13,27]. Although a major part of the cement had been resorbed and replaced by newly formed bone,

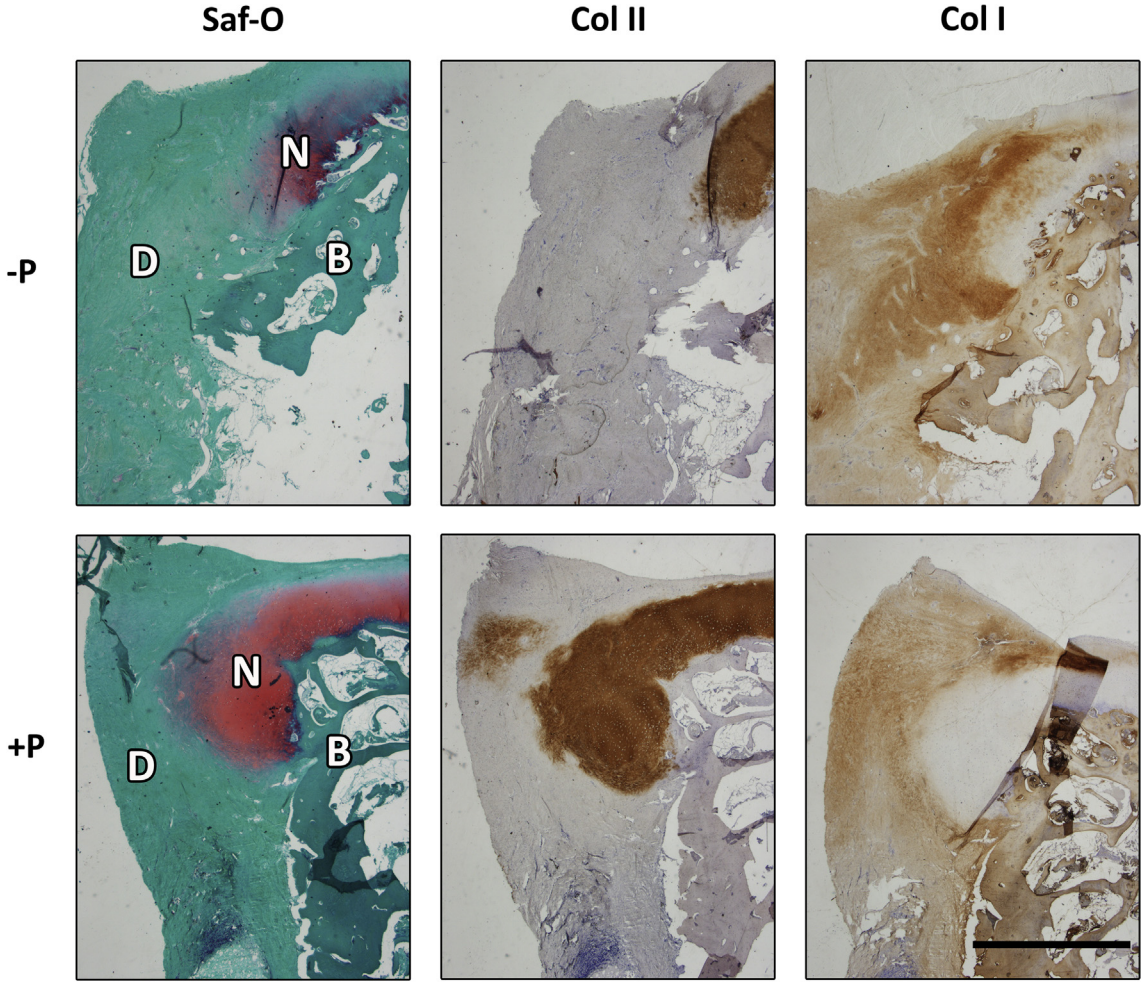

Fig. 7. Histological evaluation of the composition of the repair tissue after 6 months. Positive safranin-O staining (red) was predominantly observed at the edges of the defect, and co-localized with the immunolocalisation of collagen type II (brown). Immunolocalisation of collagen type I (brown) was homogeneous in the fibrous repair tissue. Scale bar represents 2 mm.

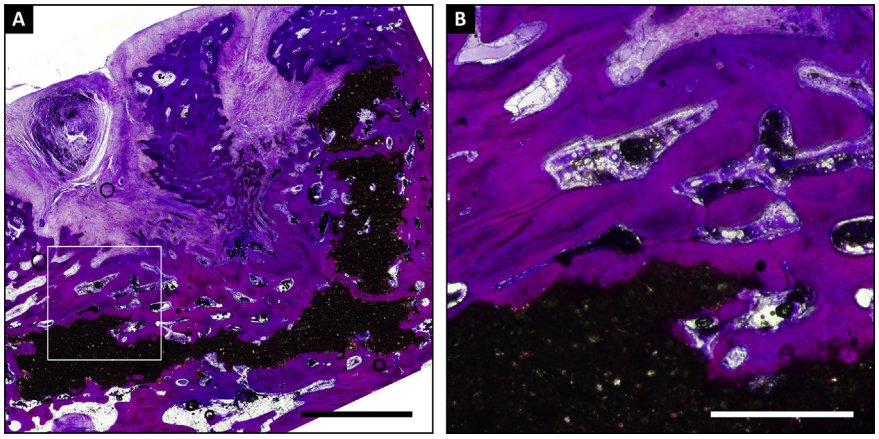

Fig. 8. MMA embedded section of a defect with a scaffold with a CaP base (+P) stained with methylene blue/basic fuchsine. The overview (A) shows substantial retention of the scaffold (in black) that is well connected to the bone, as shown by higher magnification (B). Scale bars represent 3 mm (A) and 1 mm (B).

remaining fragments were still visible within the implantation site. X-ray diffraction (XRD) analysis clearly confirmed that brushite and monetite as main components of the scaffolds were fully resorbed and only a minor amount of residual β-TCP could be found, likely due to the lower solubility of β-TCP (~0.4 mg/l) compared to brushite (85 mg/l) and monetite (41 mg/l)[28]. All diffraction patterns revealed nanocrystalline HA as the major component given the broad peaks around 2Theta = 25.8° and 31–35°. This HA might be formed either directly after scaffold implantation from hydrolysis of α-TCP to calcium deficient HA[29], or after longer times by the conversion of brushite into HA in the presence of Ca^{2+}. The latter often appears for brushite based biocements following orthotopic implantation[30], as the compound is thermodynamically instable at physiological pH values. Since the lateral resolution of the used XRD is in the order of several mm^2, the HA may also stem from newly formed bone mineral next to the scaffold residues.

Several factors may have contributed to the limited performance of the implants in the long-term study. In decellularized scaffolds the efficacy of the decellularization process is known to affect the host response and *in vitro* more aggressive decellularization was associated with a shift in macrophage phenotype predominance from M1 to M2[31]. Although not well researched, the clinical impression among veterinarians exists that the horse is a relatively sensitive animal to immunogenic stimuli compared to other species, which may also have affected the fate of the implanted scaffolds in this study. Another potentially very important factor is the initial biomechanical loading, both shear and compression, the implanted scaffolds have been subjected to from the very moment the horses recovered from anaesthesia. This is a well-known drawback of the equine model[25], which is due to the inability of the horse to unload one of its limbs for any prolonged period of time without severe complications. Additionally, the limited overall mechanical properties of the CDM scaffold may have contributed to failure by hampering the transfer of the forces to the underlying bone, ultimately resulting in bone loss in these regions. This stresses the need for more mechanically stable, e.g., fibre-reinforced constructs[32,33], for the treatment of defects in these mechanically challenging locations.

Outcomes might also further have been improved by the inclusion of regenerative cells to further enhance the tissue formation. However, this will be a complicating factor when an off-the-shelf solution, i.e., a cell-free construct, is envisioned.

Taken together, the poor outcomes of the long-term equine study were not in line with the observed promising results of the *in vitro*, ectopic *in vivo* and the short-term *in vivo* pilot studies. Where the horses did clinically surprisingly well with exhibition of relatively mild lameness only, in the long-term study very limited defect filling was observed compared to the outcomes of the 8-week pilot study. This study thus underscores the need for long-term studies in a challenging model when evaluating regenerative approaches to treat joint defects, even if the outcome of *in vitro* work and even short-term *in vivo* studies may be promising, as the performance of treatments may otherwise be overestimated. The outcome also suggests there may be substantial added value of more and more in-depth monitoring during long-term studies, for example, through imaging technologies or advanced profiling of the synovial fluid composition.

Author contributions

R.V.B., S.M.C., K.E.M.B., U.G., R.W. and J.M. contributed to the conception and design of the study. R.V.B., S.M.C., J.E.E.M., K.E.M.B., S.G.P., and J.M. performed the experiments. R.V.B., S.M.C., K.E.M.B., U.G., S.G.P., H.W., J.G., R.W. and J.M. contributed to the analysis and interpretation of data. All approved the submitted manuscript.

Conflict of interest

The authors have nothing to disclose.

Acknowledgements

The authors thank W. Boot and M. van Rijen for their assistance with scaffold preparation and histology and P. Moshtagh for assistance with the biomechanical testing. The primary antibody against collagen type II (II-II6B3), developed by Linsenmayer, was obtained from the DSHB. The research leading to these results has received funding from the Ministerio de Ciencia, Tecnología y Telecomunicaciones de Costa Rica (MICITT), the Consejo Nacional para Investigaciones Científicas y Tecnológicas de Costa Rica (CONICIT), the European Community's Seventh Framework Programme (FP7/2007–2013) under grant agreement no. 309962 (HydroZONES), the European Research Council under grant agreement 647426 (3D-JOINT), and the Dutch Arthritis Foundation (LLP-12 and LLP-22).

Supplementary data

Supplementary data related to this article can be found at http://dx.doi.org/10.1016/j.joca.2016.08.005.

References

1. Richter DL, Schenck Jr RC, Wascher DC, Treme G. Knee articular cartilage repair and restoration techniques: a review of the literature. Sports Health 2016;8:153–60.
2. Bekkers JE, Creemers LB, Tsuchida AI, van Rijen MH, Custers RJ, Dhert WJ, *et al*. One-stage focal cartilage defect treatment with bone marrow mononuclear cells and chondrocytes leads to better macroscopic cartilage regeneration compared to microfracture in goats. Osteoarthritis Cartilage 2013;21:950–6.
3. Wiegant K, van Roermund PM, Intema F, Cotofana S, Eckstein F, Mastbergen SC, *et al*. Sustained clinical and structural benefit after joint distraction in the treatment of severe knee osteoarthritis. Osteoarthritis Cartilage 2013;21:1660–7.
4. Badylak SF. The extracellular matrix as a biologic scaffold material. Biomaterials 2007;28:3587–93.
5. Crapo PM, Gilbert TW, Badylak SF. An overview of tissue and whole organ decellularization processes. Biomaterials 2011;32:3233–43.
6. Gawlitta D, Benders KE, Visser J, van der Sar AS, Kempen DH, Theyse LF, *et al*. Decellularized cartilage-derived matrix as substrate for endochondral bone regeneration. Tissue Eng Part A 2015;21:694–703.
7. Benders KE, Boot W, Cokelaere SM, Van Weeren PR, Gawlitta D, Bergman HJ, *et al*. Multipotent stromal cells outperform chondrocytes on cartilage-derived matrix scaffolds. Cartilage 2014;5:221–30.
8. Visser J, Gawlitta D, Benders KE, Toma SM, Pouran B, van Weeren PR, *et al*. Endochondral bone formation in gelatin methacrylamide hydrogel with embedded cartilage-derived matrix particles. Biomaterials 2015;37:174–82.
9. Kang H, Peng J, Lu S, Liu S, Zhang L, Huang J, *et al*. In vivo cartilage repair using adipose-derived stem cell-loaded decellularized cartilage ECM scaffolds. J Tissue Eng Regen Med 2014;8:442–53.
10. Yang Z, Shi Y, Wei X, He J, Yang S, Dickson G, *et al*. Fabrication and repair of cartilage defects with a novel acellular cartilage matrix scaffold. Tissue Eng Part C Methods 2010;16:865–76.
11. Panseri S, Russo A, Cunha C, Bondi A, Di Martino A, Patella S, *et al*. Osteochondral tissue engineering approaches for articular cartilage and subchondral bone regeneration. Knee Surg Sports Traumatol Arthrosc 2012;20:1182–91.
12. Benders KE, van Weeren PR, Badylak SF, Saris DB, Dhert WJ, Malda J. Extracellular matrix scaffolds for cartilage and bone regeneration. Trends Biotechnol 2013;31:169–76.
13. Habibovic P, Gbureck U, Doillon CJ, Bassett DC, van Blitterswijk CA, Barralet JE. Osteoconduction and osteoinduction of low-temperature 3D printed bioceramic implants. Biomaterials 2008;29:944–53.
14. Gbureck U, Vorndran E, Muller FA, Barralet JE. Low temperature direct 3D printed bioceramics and biocomposites as drug release matrices. J Control Release 2007;122:173–80.
15. McIlwraith CW, Fortier LA, Frisbie DD, Nixon AJ. Equine models of articular cartilage repair. Cartilage 2011;2:317–26.
16. Moran CJ, Ramesh A, Brama PA, O'Byrne JM, O'Brien FJ, Levingstone TJ. The benefits and limitations of animal models for translational research in cartilage repair. J Exp Orthop 2016;3:1.
17. McIlwraith CW, Robertson JT. Equine Surgery. Advanced Techniques. William & Wilkins; 1998.
18. Pathak S, Kalidindi SR. Spherical nanoindentation stress–-strain curves. Mater Sci Eng Rep 2015;91:1–36.
19. Jin H, Lewis JL. Determination of Poisson's ratio of articular cartilage by indentation using different-sized indenters. J Biomech Eng 2004;126:138–45.
22. Vacanti CA. The history of tissue engineering. J Cell Mol Med 2006;10:569–76.
23. Hurtig MB, Buschmann MD, Fortier LA, Hoemann CD, Hunziker EB, Jurvelin JS, *et al*. Preclinical studies for cartilage repair: recommendations from the international cartilage repair society. Cartilage 2011;2:137–52.
24. Malda J, Benders KE, Klein TJ, de Grauw JC, Kik MJ, Hutmacher DW, *et al*. Comparative study of depth-dependent characteristics of equine and human osteochondral tissue from the medial and lateral femoral condyles. Osteoarthritis Cartilage 2012;20:1147–51.
25. Ahern BJ, Parvizi J, Boston R, Schaer TP. Preclinical animal models in single site cartilage defect testing: a systematic review. Osteoarthritis Cartilage 2009;17:705–13.
26. Williams RB, Harkins LS, Hammond CJ, Wood JL. Racehorse injuries, clinical problems and fatalities recorded on British racecourses from flat racing and National Hunt racing during 1996, 1997 and 1998. Equine Vet J 2001;33:478–86.
27. Tamimi F, Torres J, Al-Abedalla K, Lopez-Cabarcos E, Alkhraisat MH, Bassett DC, *et al*. Osseointegration of dental implants in 3D-printed synthetic onlay grafts customized according to bone metabolic activity in recipient site. Biomaterials 2014;35:5436–45.
28. Holzapfel BM, Reichert JC, Schantz JT, Gbureck U, Rackwitz L, Noth U, *et al*. How smart do biomaterials need to be? A translational science and clinical point of view. Adv Drug Deliv Rev 2013;65:581–603.
29. Carrodeguas RG, De Aza S. alpha-Tricalcium phosphate: synthesis, properties and biomedical applications. Acta Biomater 2011;7:3536–46.
30. Kanter B, Geffers M, Ignatius A, Gbureck U. Control of in vivo mineral bone cement degradation. Acta Biomater 2014;10:3279–87.
31. Keane TJ, Londono R, Turner NJ, Badylak SF. Consequences of ineffective decellularization of biologic scaffolds on the host response. Biomaterials 2012;33:1771–81.
32. Visser J, Melchels FP, Jeon JE, van Bussel EM, Kimpton LS, Byrne HM, *et al*. Reinforcement of hydrogels using three-dimensionally printed microfibres. Nat Commun 2015;6:6933.
33. Boere KW, Visser J, Seyednejad H, Rahimian S, Gawlitta D, van Steenbergen MJ, *et al*. Covalent attachment of a three-dimensionally printed thermoplast to a gelatin hydrogel for mechanically enhanced cartilage constructs. Acta Biomater 2014;10:2602–11.